Materials Research. 2025; 28: e20250640
DOI: https://doi.org/10.1590/1980-5373-MR-2025-0640

CC BY

Enhancing Mechanical and Structural Properties of PLA/Wood Composites Through Annealing

Frederico de Castro Magalhães[a]*, **Claudia V. Campos Rubio[a]**, **Juan Carlos Campos Rubio[a]**

[a]*Universidade Federal de Minas Gerais, Departamento de Engenharia Mecânica, Av. Antonio Carlos, 6627, Campus Pampulha, 31270-901, Belo Horizonte, MG, Brasil.*

Received: September 15, 2025; Revised: November 21, 2025; Accepted: November 29, 2025

This study examines the effect of heat treatment at 50 °C on PLA/Wood composites produced by fused deposition modelling (FDM). The material consisted of PLA with 20 wt% recycled pine particles and was printed in two raster orientations (0°/90° and −45°/45°). Annealing was performed at 50 °C for 1 h, below the glass transition region, to promote molecular relaxation at interlayer regions while preserving dimensional stability. After treatment, the void content decreased from ~12.7% to ~11.4%, and Shore D hardness increased by ~2%. Tensile strength rose from 17.83 to 28.95 MPa (0°/90°) and from 16.55 to 27.58 MPa (−45°/45°). Flexural strength increased by up to 48%, and Charpy impact resistance increased from 34.36 to 48.86 kJ/m^2 (0°/90°) and from 42.23 to 54.38 kJ/m^2 (−45°/45°). Microscopy indicated reduced interlayer separation and more cohesive fracture paths after annealing. The results show that heat treatment at 50 °C improves mechanical performance in PLA/Wood without altering external geometry or compromising the bio-based reinforcement.

Keywords: *Additive Manufacturing, PLA/Wood Composite, Annealing Treatment, Mechanical Properties.*

1. Introduction

Additive manufacturing using Fused Deposition Modeling (FDM) is recognized as one of the most accessible and popular techniques for 3D object printing[1]. This method involves extruding polymer filaments and depositing them layer by layer, enabling the production of functional parts with complex geometries. Its simplicity makes FDM versatile for a variety of polymers, provided that parameters such as printing speed, temperature, and retraction are adequately controlled[2].

Polylactic acid (PLA) is a biodegradable thermoplastic derived from renewable sources such as corn starch or sugarcane[3]. In FDM processing, PLA exhibits stable extrusion behavior and does not require high processing temperatures, typically between 190 °C and 220 °C. Its density ranges from 1.24 to 1.26 g cm^{-3}, tensile strength from 38 to 55 MPa, and elastic modulus from 3.0 to 3.6 GPa, depending on the printing parameters and raster orientation. However, its relatively low elongation at break (3–8%) and heat deflection temperature (~ 55–60 °C) limit its application in load-bearing or thermally exposed components[4].

To overcome these limitations, several composite filaments have been developed by combining PLA with different reinforcements, such as carbon fibers (PLA/CF), glass fibers (PLA/GF), and lignocellulosic particles (PLA/Wood). PLA/CF and PLA/GF composites exhibit increased stiffness and strength due to the high modulus of the reinforcing fibers, with tensile strength values reaching approximately 42 MPa under optimized printing parameters[5]. However, these reinforcements reduce biodegradability and increase material cost. In contrast, PLA/Wood composites incorporate renewable lignocellulosic residues composed mainly of cellulose, hemicellulose, and lignin, providing a sustainable route to enhance stiffness and reduce density without compromising environmental compatibility. Siddiqui et al.[6] reported that a PLA/wood-fiber composite containing 20 wt% reinforcement achieved a tensile strength of about 50 MPa and a flexural strength of 94 MPa, demonstrating that natural lignocellulosic fillers can improve mechanical performance while maintaining biodegradability.

The incorporation of wood particles into PLA is aligned with material reuse practices, since these particles generally originate from residues of the wood-processing industry. Their use reduces the volume of waste directed to landfills and allows the production of filaments based on renewable and biodegradable constituents[7,8]. This approach is consistent with circular economy principles, in which discarded lignocellulosic material is reintroduced into the production chain, contributing to the environmental relevance of PLA/Wood composites in additive manufacturing.

PLA/Wood is produced by combining a PLA matrix with wood particles, typically in concentrations between 10 wt% and 45 wt%[9]. These particles are commonly obtained from recycled lignocellulosic residues and contribute to material reutilization. Their presence affects the mechanical behavior of the composite: particle size distribution, aspect ratio, and dispersion influence stiffness, while irregular or coarser particles can act as stress concentration sites, reducing tensile strength and ductility. Additionally, under controlled

*e-mail: fredmag@demec.ufmg.br
Associate Editor: Rodrigo Orefice.
Editor-in-Chief: Luiz Antonio Pessan.

industrial composting conditions, both PLA and the wood fraction can undergo biodegradation, resulting in water, carbon dioxide, and biomass[10].

This composite has been used in components where the visual texture and tactile characteristics of wood are of interest, such as architectural models, furniture elements, and decorative items produced by additive manufacturing[11]. In these applications, processing feasibility is combined with the ability to incorporate recycled material streams. However, the heterogeneous structure resulting from the inclusion of wood particles introduces discontinuities at the particle–matrix interface, which can reduce load-transfer efficiency and mechanical stability under service conditions. Therefore, strategies that improve interfacial bonding and reduce internal voids are relevant for achieving mechanical response with reduced variability.

When compared to pure PLA, PLA/Wood composites present lower mechanical performance due to the hydrophilic–hydrophobic mismatch between the lignocellulosic particles and the PLA matrix. PLA processed by FDM shows tensile strength values in the range of 38–55 MPa, depending on raster orientation and printing parameters, whereas PLA/Wood with ~20 wt% wood particles exhibits tensile strengths between 15–30 MPa[12]. This reduction is associated with stress concentrations arising from irregular particle geometry and with limited stress transfer at the particle–matrix interface. The extrusion of the composite filament and the layer-by-layer deposition inherent to FDM introduce internal voids, which limit interlayer adhesion and result in anisotropic mechanical response.

The hygroscopic character of the wood particles also affects long-term performance. Moisture uptake can induce localized swelling and interfacial debonding, promoting microcrack formation and reducing stiffness under tensile or bending loading. Studies have shown that the absorption of moisture in natural-fiber composites can reduce tensile strength by up to approximately 40% and the elastic modulus by 20–30%, mainly due to swelling-induced stresses at the matrix–particle interface[12]. The lower thermal stability of lignocellulosic particles relative to PLA may also influence the material response during processing or service at moderate temperatures. Furthermore, the sorption behavior of wood-derived particles is anisotropic and leads to dimensional instability when exposed to humidity, which compromises interlayer cohesion in printed composites[13]. Consequently, improving adhesion between the matrix and wood particles, as well as reducing internal porosity, is essential to ensure stable mechanical performance and long-term durability.

In FDM processing, the layer-wise deposition generates a heterogeneous and anisotropic microstructure, with mechanical properties that differ from bulk-processed materials due to voids and imperfect interlayer bonding[14,15]. For PLA/Wood composites, the presence of rigid or irregular lignocellulosic particles further intensifies this anisotropy by introducing additional interfaces and stress concentration sites. Strategies that improve interlayer cohesion and reduce void content are therefore essential to obtain more reliable structural performance in such materials.

Printing parameters influence the microstructure formed during FDM processing. Lower printing speeds promote more consistent filament deposition and more continuous contact between adjacent layers, which reduces the formation of interlayer voids. Le Duigou et al.[16] reported that printing at 30 mm/s increased part density and tensile strength in comparison with speeds between 50 and 70 mm/s. Similarly, Kariz et al.[17] showed that reducing speed and adjusting layer height contributed to more uniform layer deposition in PLA/Wood composites. The characteristics of the wood particles also affect mechanical behavior: elongated or irregular particles may introduce localized stress concentrations, whereas smaller particles with more uniform dispersion within the PLA matrix tend to support a more homogeneous stress distribution during loading[12].

Research by Kariz et al.[17] showed that increasing the wood particle content from 10% to 50% reduced the tensile strength of PLA/Wood composites from 57 MPa to 30 MPa. Higher particle contents were also associated with a decrease in ductility and increased surface roughness. In addition, Le Duigou et al.[16] reported that the printing raster orientation influences the mechanical response, with specimens printed at 0°/90° reaching tensile strengths of up to 30 MPa, 20% higher than those printed at 90°. These results indicate that both the amount of wood particles and the selection of printing orientation are relevant variables when aiming to control the mechanical performance of PLA/Wood composites.

Previous studies on the annealing of PLA and PLA-based composites have predominantly examined temperatures above the glass transition region of PLA (typically between 70 °C and 120 °C) to enhance stiffness and mechanical strength. For instance, Kartal and Kaptan[18] reported a 48% increase in tensile strength and a 78% rise in elastic modulus for PLA annealed at 85 °C for 90 min (Polymer Testing, 126, 108343). Similarly, Jayanth et al.[19] observed a 35% increase in tensile strength and a 40% reduction in void content after annealing at 120 °C for 240 min. However, these post-processing temperatures often induce dimensional distortions due to the mismatch in thermal expansion coefficients between adjacent layers. In PLA/Wood composites, this issue is compounded by the lower thermal stability of the lignocellulosic fraction, as degradation and color darkening have been observed near 100 °C[6]. Therefore, annealing below the glass transition temperature—particularly near 50 °C—represents an underexplored regime that may improve interlayer adhesion and stress relaxation without compromising geometric stability or particle integrity.

In this study, the effect of annealing at 50 °C on PLA/Wood composites produced by fused deposition modelling was examined. The selected temperature is below the softening range of the PLA/Wood composite, which limits dimensional changes while allowing partial relaxation of internal stresses and improved contact between adjacent layers. The specimens were annealed under sand confinement to ensure uniform heat transfer and to maintain geometric stability during heating. Mechanical tests in tension, flexure and impact were used to quantify the influence of annealing on structural performance, and microscopy was employed to assess interlayer cohesion and the interaction between the polymer matrix and wood particles. This approach provides a post-processing route aimed at improving the mechanical performance of PLA/Wood components without altering the printable nature or composition of the material.

2. Materials and Methods

To accomplish the objectives of this research, a structured experimental plan was established, as illustrated in Figure 1. A commercial PLA/Wood filament containing approximately 20 wt% recycled pine particles was used to fabricate 3D-printed specimens by fused deposition modeling (FDM). The specimens were printed for tensile, flexural, and impact testing, following the respective ASTM standards: D638 (tensile), D5045-14 (four-point bending), and D6110 (Charpy impact). After printing, the specimens were subjected to a thermal treatment at 50 °C for 1 h under sand confinement to ensure uniform heating and dimensional stability. Subsequently, the printed parts were evaluated in terms of dimensional accuracy, Shore D hardness, tensile and flexural strength, and impact energy absorption. Additional tensile tests were also performed on the filaments themselves, with and without annealing, to assess the direct influence of heat treatment on the material prior to printing.

2.1. Materials

The material used in this study was a commercially available composite filament labeled PLA/Wood, comprising 80 wt% PLA and 20 wt% recycled pine wood particles. The wood particles featured irregular shapes and dimensions ranging between 0.25 and 0.35 mm. The choice of a 20% wood particle composition reflects practical limitations, as higher concentrations (near 40%) can lead to processing difficulties such as percolation effects, flow instability, and nozzle blockages. The filament, manufactured by Volt3D (Volt3D, Santo André, São Paulo, Brazil), exhibited an average diameter of 1.75 ± 0.03 mm (ISO 17953–1:2015). Prior to use, the filament was dried at 60 °C for 24 hours and subsequently stored in vacuum-sealed packaging to prevent moisture absorption.

The manufacturer reports a glass transition temperature (Tg) of approximately 60–65 °C and a melting temperature (Tm) in the range of 150–160 °C for the PLA matrix. The addition of lignocellulosic particles reduces the composite density compared to neat PLA and introduces internal porosity. Based on mass-to-volume density measurements carried out in this study, the PLA/Wood filament showed a density of 1.21 $g \cdot cm^{-3}$. When compared to the theoretical density estimated by the rule of mixtures for an 80 wt% PLA and 20 wt% wood composition, this value corresponds to an internal void content of approximately 12%. These microstructural features are relevant because voids and particle–matrix interfaces directly influence interlayer bonding and mechanical response in FDM-processed composites.

2.2. Process parameters

For slicing the 3D models generated in CAD software (SolidWorks 2008) into individual layers, Cura 5.2 (Creality Sunlu, China) was used. Printing was performed using a nozzle with a diameter of 0.4 mm. The manufacturer recommends nozzle temperatures between 195–220 °C and bed temperatures between 50–60 °C, with printing speeds ranging from 40–100 $mm \cdot s^{-1}$. In this study, a printing speed of 40 $mm \cdot s^{-1}$ was selected to maintain stable filament flow and to reduce the likelihood of nozzle blockage associated with the presence of wood particles in the composite filament.

A dedicated filament dryer (Creality, Sunlu, China) was used during printing to maintain the filament at 50°C and minimize moisture absorption. All specimens for mechanical testing were printed directly onto a heated bed with an adhesive coating to prevent detachment during cooling. The infill density was set to 100%, producing fully dense specimens. The detailed printing parameters used in this

Figure 1. Flowchart illustrating the research steps.

study are summarized in Table 1. All samples were printed with the XY plane aligned to the heated bed, maintaining a consistent raster deposition sequence and reducing the risk of warping or dimensional distortion during cooling.

2.3. Specimens

The printed specimens were prepared according to the geometrical specifications defined in the respective ASTM standards for each mechanical test. Tensile specimens followed ASTM D638 Type I, four-point bending specimens followed ASTM D5045-14, and Charpy impact specimens were prepared in accordance with ASTM D6110, using notched specimens. For each test configuration, five specimens were produced (n = 5) for each printing orientation (0°/90° and −45°/45°) and for both conditions (with and without annealing), in order to enable statistical comparison. All specimens were printed simultaneously to maintain identical processing conditions. Dimensional stability after annealing at 50 °C was verified by measuring length, width, and thickness using a digital caliper (Mitutoyo, model 500-196-30) with 0.001 mm resolution. Figure 2 shows the dimensions used for the tensile, flexural, and impact test specimens.

2.4. Testing equipaments

The tensile tests were performed on a Shimadzu AG-IS universal testing machine equipped with a 100 kN load cell at a crosshead speed of 3 mm/min, following the ASTM D638 Type I standard. The four-point bending tests were also carried out on the same equipment at a crosshead speed of 2 mm/min, according to ASTM D5045-14. Force and displacement data were acquired at 100 Hz and converted to stress and strain based on the measured cross-sectional dimensions and gauge lengths.

In addition to the printed specimens, separate tensile tests were performed on PLA/Wood filaments—both untreated and annealed—to evaluate the direct effect of heat treatment on the composite material prior to 3D printing. These filament tests were conducted solely for comparison and were not used to fabricate the printed specimens. Each filament segment (200 mm in length) was mounted in Bollard-style grips and loaded at 3 mm/min to determine tensile behavior and estimate void evolution independently from the printed samples.

A BOT 633 D Charpy impact tester with a maximum energy of 10 J was used to determine the impact strength (E_c) according to ASTM D6110 for 3D-printed PLA/Wood specimens, both untreated and annealed. The absorbed energy was calculated using Equation (1):

$$E_c = \frac{E_T}{wt} \quad (1)$$

where E_t is the total fracture energy, and w and t are the specimen width and thickness, respectively. Energy losses due to bearing friction and air resistance were neglected because of their negligible contribution to the energy balance. Tensile toughness was determined by integrating the stress–strain curve up to fracture, representing the total energy absorbed per unit volume ($J \cdot cm^{-3}$).

Shore D hardness was measured using a PCE-HT200 durometer (PCE Instruments), following ASTM D2240. Each specimen was tested at five equally spaced points along its central region, avoiding edges and visible pores; the reported value corresponds to the mean of the five readings.

The void content (V%) was determined by the gravimetric method in accordance with ASTM D2734. The theoretical density ($\rho_{theoretical}$) was calculated from the weighted densities of PLA ($1.24\ g \cdot cm^{-3}$) and wood particles ($0.60\ g \cdot cm^{-3}$), while the experimental density ($\rho_{measured}$) was obtained from the

Table 1. Printing Parameters Used for Specimen Fabrication.

Parameters	Values	Units
Nozzle temperature	200	[ºC]
Bed temperature	55	[ºC]
Infill line directions	[0º/90º] [-45º/45º]	[º]
Layer height	0.20	[mm]
Print speed	40	[mm/s]
Line width	0.4	[mm]
Infill density	100	%
Number of perimeters	4	Wall

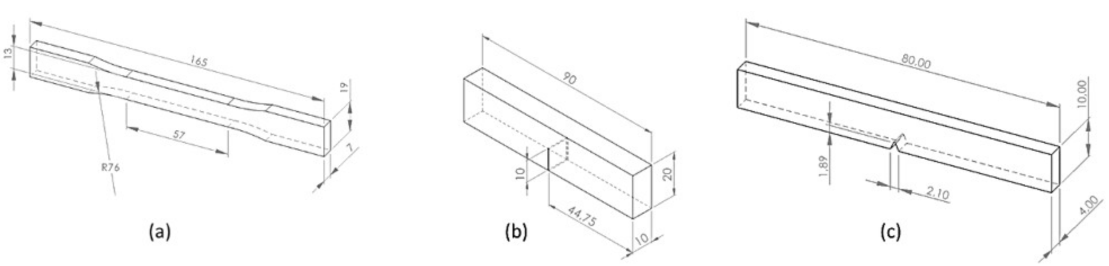

Figure 2. Dimensions (mm) of Specimens for Mechanical Testing.

mass-to-volume ratio using an Analytical Balance Sartorius Entris 224-1S (±0.1 mg). The void percentage was then calculated according to Equation (2):

$$V = \left(1 - \frac{\rho_{measured}}{\rho_{theoretical}}\right).100 \quad (2)$$

All density measurements were performed in triplicate for each printing orientation and thermal condition.

Microscopic observations were performed to correlate mechanical performance with printed morphology. Optical images were acquired using a Leica DM750M microscope (Leica Microsystems) equipped with a digital camera. The fracture surfaces and visible cross-sections of the specimens were examined in the as-fractured condition, without additional cutting or polishing, to prevent artefacts at the polymer–wood interface. The analyses focused on interlayer voids, filament interfaces, matrix–particle contact, and fracture-path continuity, comparing untreated and annealed samples for both raster orientations.

All tests were carried out at room temperature (24 ± 2 °C) and 50 ± 5% relative humidity.

2.5. Annealing heat treatment

PLA/Wood filaments and printed specimens were subjected to annealing at 50 °C for 1 hour, followed by cooling to room temperature. Figure 3 shows specimens were placed in rectangular aluminum trays and fully embedded in 2 cm of fine dune sand (particle size ~ 0.074 mm), with an additional 2 cm of sand covering the top surface. The sand layer ensured uniform heat transfer and applied a low and evenly distributed surface pressure (~490 Pa) that helped prevent geometric distortion during heating.

Following annealing, dimensional stability was verified by measuring specimen length, width, and thickness using a digital caliper with 0.001 mm resolution, and no dimensional changes were observed. This confirms that the sand layer did not induce mechanical compaction or densification of the printed structure, indicating that the observed property changes arise from the thermal treatment itself rather than from physical confinement.

Shore D hardness measurements were performed on the printed surfaces to evaluate changes in surface rigidity after annealing. At 50 °C, the treatment is expected to promote polymer chain relaxation and enhanced interlayer contact, without inducing substantial changes in crystallinity, since the temperature remains below the effective crystallization range of PLA. Thus, the observed variations in hardness are primarily attributed to improved interfacial consolidation rather than structural reorganization of the crystalline phase.

3. Results and Discussion

3.1. Analysis of filaments

Annealing thermal treatment was applied to PLA/Wood filaments, followed by thermogravimetric and tensile tests performed both before and after treatment. The thermogravimetric analysis evaluated the influence of annealing on the wood particle content in the PLA/Wood filament, which contains 20 wt% according to the manufacturer. Figure 4a graphically displays the thermogravimetric test results for PLA/Wood filaments, while Figure 4b presents the tensile test results for the filament with and without annealing at 50°C.

Thermogravimetric analysis (Figure 4a) was performed to evaluate the thermal stability of the PLA/Wood filament and to confirm the wood particle content. The composite exhibited a main degradation region between 300 °C and 400 °C, associated with the decomposition of both the PLA matrix and the lignocellulosic constituents of the recycled pine wood particles. The final residue of approximately 17 wt% is consistent with the nominal composition reported by the manufacturer, indicating that the annealing process at 50 °C did not induce mass loss or thermal degradation of the reinforcing phase.

The incorporation of wood particles reduces the onset temperature of thermal degradation. This effect is associated with the decomposition of cellulose, hemicellulose and lignin, which begins in the range of 200–300 °C. Therefore, the thermal stability of PLA/Wood is limited by the thermal response of the lignocellulosic phase, which degrades earlier than the PLA matrix.

Figure 4b presents the tensile test results for the PLA/Wood filament before and after annealing at 50 °C. A modest increase in maximum tensile stress (approximately 10%)

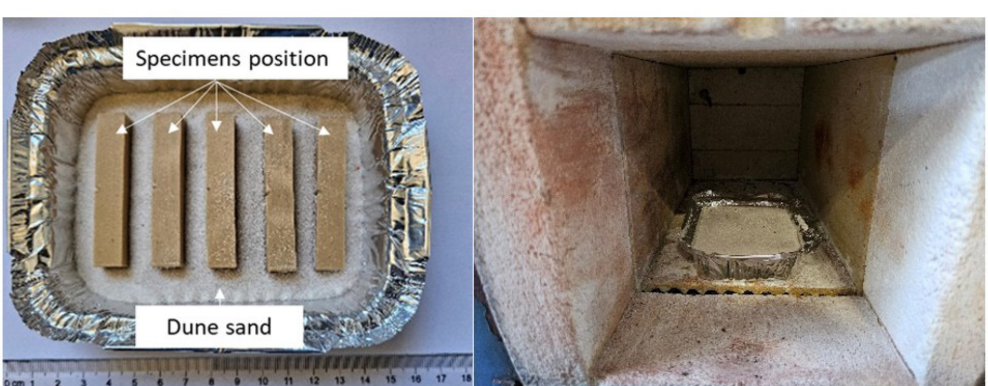

Figure 3. Specimen Placement for Hardness Testing and Annealing Process (a) Initial layer of sand positioning. (b) Specimen fully covered with sand inside the oven.

was recorded after annealing, associated with polymer chain relaxation and reduction of residual stresses generated during filament extrusion. Issametova et al.[20] reported similar behavior, where post-processing heat treatment effectively relieved FDM-induced internal stresses and increased tensile performance. This trend is consistent with the study of Suder et al.[21] which reported an ~ 9–10% increase in tensile strength after controlled annealing of PLA. At 50 °C — slightly below the glass transition temperature of PLA (~ 55–65 °C) — chain mobility enables localized rearrangement within the amorphous phase. Kartal and Kaptan[18] demonstrated that annealing below Tg can activate constrained segmental motions without phase transformation, improving stress transfer across amorphous regions.

Regarding the strain behavior, the annealed PLA/Wood50 filament did not exhibit a reduction in deformation capacity. Instead, the strain response became more uniform, indicating a reduction in internal stress gradients and improved compatibility at the PLA–wood particle interfaces. Comparable interface improvements have been observed in wood-filled PLA composites subjected to mild thermal treatment, as reported by Tomec et al.[22], where thermally modified wood particles enhanced particle–matrix adhesion and reduced porosity. Because the treatment temperature remains below the glass transition range of the PLA/Wood system, the supplied thermal energy is insufficient to promote any crystalline phase development. Therefore, the mechanical changes observed after annealing are better interpreted as stress relaxation and increased molecular packing density within interlayer regions, rather than as crystallization processes. A similar interpretation was presented in the study by Fouly et al.[23] indicating that moderate annealing enhances structural stability by reducing residual stress without inducing brittle behavior.

Optical micrographs of fracture cross-sections (Figure 5) reveal globular internal voids in the untreated PLA/Wood filament, likely associated with incomplete wetting of wood particles and porosity resulting from extrusion. After annealing at 50 °C, a reduction in the size and distribution of voids is observed. The slight increase in chain mobility at this temperature allows the matrix to adapt locally to the particle surfaces, improving interfacial contact.

Comparing the composite PLA/Wood filament (Figure 5b), it is evident that it exhibits internal porosity, predominantly

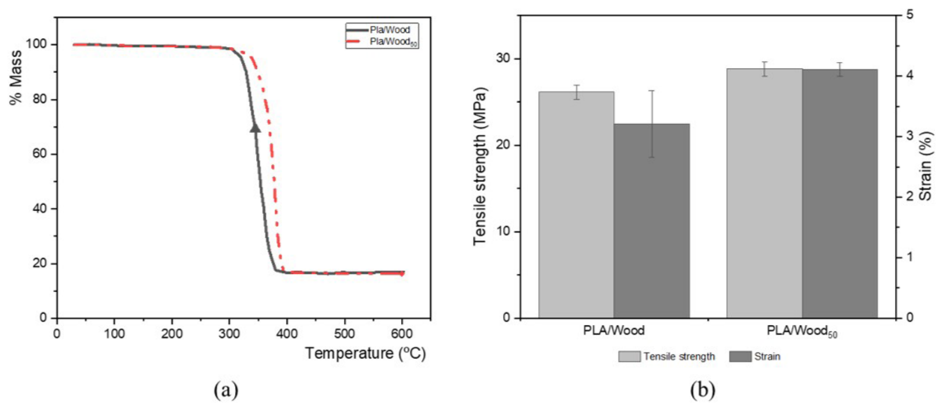

Figure 4. Effects of Annealing on PLA/Wood Filament. (a) Thermogravimetric analysis results for PLA/Wood filament. (b) Tensile test results for PLA/Wood filaments with and without annealing.

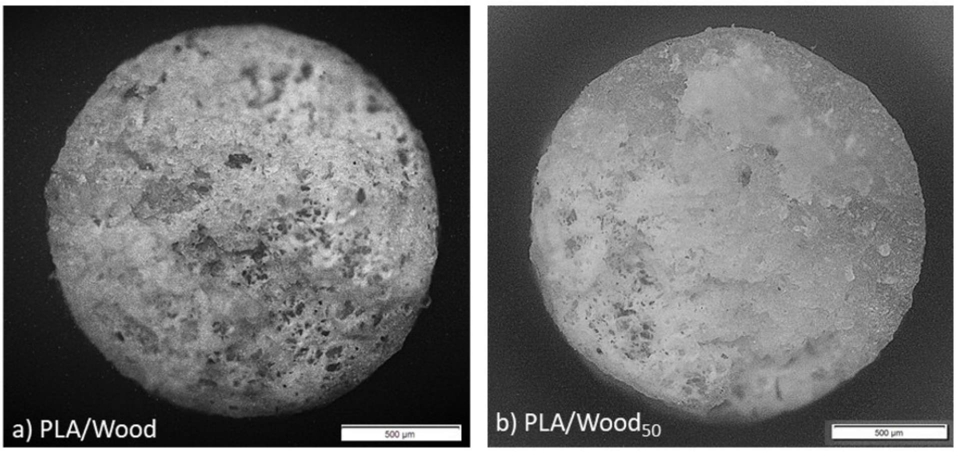

Figure 5. Optical micrographs of fracture cross-sections of the filaments after tensile testing. (a) (a) PLA/Wood, (b) PLA/Wood$_{50}$.

globular in shape, located within the fracture region. This porosity pattern is also observed in the thermally treated PLA/Wood filaments and may be attributed to incomplete wetting of the PLA matrix around the irregular wood particles, combined with intrinsic voids generated during filament extrusion. In the annealed PLA/Wood$_{50}$ condition, a reduction in the size and distribution of these voids is observed. At 50 °C, slight molecular mobility allows localized chain relaxation and improved interfacial accommodation between the PLA matrix and the wood particle surfaces. This temperature therefore appears to promote a more uniform internal structure, improving stress transfer and contributing to the enhanced mechanical performance of the filament after annealing. A similar reduction in pore size and improved particle–matrix adhesion was reported in the study by Tomec et al.[22], indicating that the thermal modification of wood particles enhances interfacial compatibility and reduces overall porosity in PLA/wood composites.

3.2. *Evaluation of tensile properties before and after annealing*

Before the tensile tests, Shore D hardness and void percentage were evaluated in the 3D-printed PLA/Wood specimens to assess the influence of annealing on densification and structural cohesion. Figure 6 presents the hardness values and void fractions for both printing orientations. The untreated specimens exhibited hardness values of 77.5 for the 0°/90° orientation and 75.5 for the −45°/45° orientation. The slightly higher hardness in the 0°/90° configuration, representing a 2.6% difference, is consistent with the alignment of filament strands along the loading direction, which promotes higher resistance to local indentation and contributes to greater surface rigidity.

After annealing at 50 °C, the hardness of the PLA/Wood specimens increased to 78.8 for the 0°/90° orientation and 76.6 for the −45°/45° orientation, corresponding to increases of +1.7% and +1.5%, respectively, relative to the untreated condition. This improvement reflects increased interlayer cohesion and reduced void content, resulting from polymer-chain relaxation and local molecular rearrangement at temperatures near the glass transition of PLA. Because the treatment temperature remains below Tg, the observed changes are attributed primarily to stress relaxation and improved packing within the amorphous phase.

The void percentages followed a similar trend. Untreated PLA/Wood specimens exhibited void contents of 12.42% (0°/90°) and 12.77% (−45°/45°), indicating incomplete interlayer fusion and entrapped porosity associated with the presence of irregular wood particles. After annealing, void content decreased to 11.48% and 11.42%, corresponding to reductions of 7.6% and 10.6%, respectively. These reductions demonstrate that localized chain mobility at 50 °C enables the partial collapse or accommodation of small voids, improving the continuity of the printed layers. This effect also narrows the difference in structural density between the two printing orientations, indicating a more homogeneous interlayer compaction after annealing. Comparable reductions in porosity and enhancement of interlayer bonding following moderate heat treatment were reported in the study by Tomec et al.[22], where thermally modified wood-particle PLA composites exhibited reduced pore volume and improved interfacial densification. The Figure 7 shows the results for Young's modulus, tensile strength, and strain obtained from tensile tests of PLA/Wood specimens printed in different raster orientations, with and without annealing at 50 °C.

The tensile behavior of the PLA/Wood composite demonstrated clear differences between the untreated and annealed conditions. The Young's modulus increased from 3.23 GPa to 3.41 GPa in the 0°/90° orientation (+5.6%) and from 3.05 GPa to 3.21 GPa in the −45°/45° orientation (+5.2%). This increase reflects stress relaxation and improved cohesion at interlayer regions, which promote more uniform load transfer during tensile loading. Similar strengthening trends were reported in the study by Kahya et al.[24], demonstrating that heat treatment near the glass-transition temperature enhances interlayer diffusion and significantly increases the elastic modulus of FDM-printed PLA. The smaller difference between orientations after annealing indicates partial homogenization of the mechanical response, consistent with the reduced void content observed microscopically.

The tensile strength increased after annealing at 50 °C, from 17.83 MPa to 28.95 MPa in the 0°/90° specimens (+62.4%) and from 16.55 MPa to 27.58 MPa in the −45°/45° configuration (+66.6%). The improvement results from enhanced interlayer bonding and reduced interfacial gaps, which allow

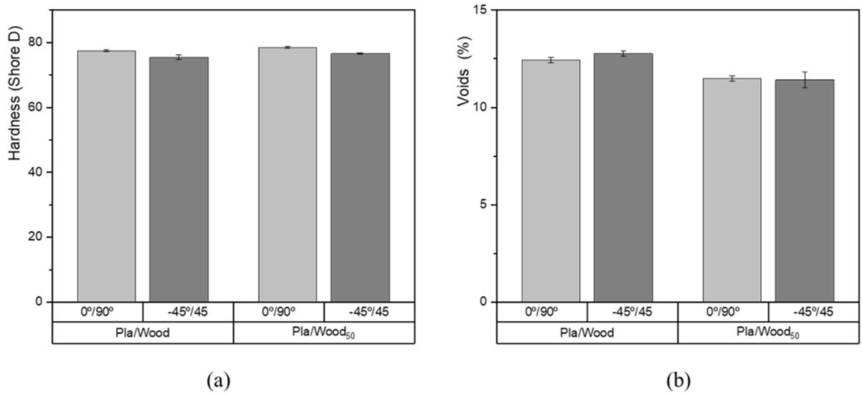

Figure 6. Shore D Hardness and void percentage of 3D-printed specimens.

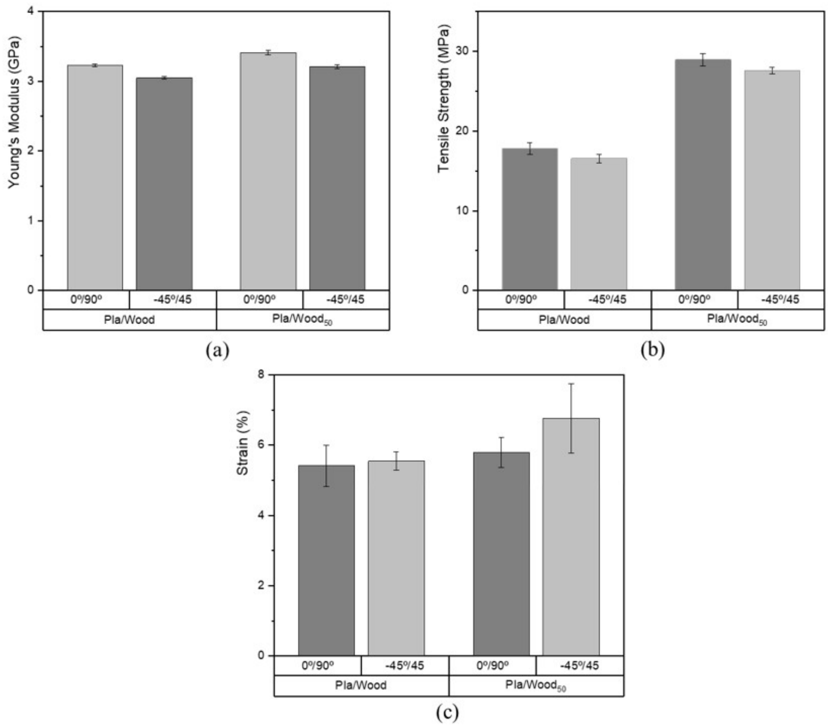

Figure 7. Results of (a) Young's Modulus, (b) Tensile Strength and (c) Strain from Tensile Tests.

tensile loads to be transmitted through the deposited filaments without premature separation between layers. Comparable findings were reported by Natayu et al.[25], indicating that annealing improved tensile strength by over 60% owing to reduced internal voids and enhanced cohesion between adjacent filament layers. Since the treatment temperature is below the transition range of the PLA/Wood composite, the strengthening is attributed to localized molecular relaxation and densification at the interlayer regions, which increase cohesion and reduce residual stress gradients.

The strain at maximum load increased in the 0°/90° orientation from 0.0561 to 0.0598 (+6.6%) and in the −45°/45° orientation from 0.0579 to 0.0679 (+17.2%). The larger increase in the inclined raster configuration results from shear transfer across interlayer planes, where tensile load is supported by the integrity of the filament interfaces. The reduction in void connectivity and the consolidation of interlayer contact after annealing allowed deformation to extend through the deposited filaments instead of concentrating at weak boundaries. These results are consistent with the mechanisms described in the study by Shbanah et al.[26], indicating that heat-treated PLA exhibits improved strain uniformity due to enhanced interlayer adhesion and reduced stress concentration at filament boundaries. This increased cohesion promotes a more stable distribution of deformation within the composite.

Figure 8 presents cross-sectional views of the fracture regions of the tensile specimens for PLA/Wood filaments, both with and without heat treatment, highlighting the differences between the 0º/90º and -45º/45º printing orientations.

Changes in fracture morphology are consistent with the mechanical responses obtained. In the untreated specimens, the fracture path followed the boundaries between adjacent deposited filaments, indicating separation along interlayer regions. After annealing, the fracture surfaces for both printing orientations showed reduced separation between layers. In the 0°/90° configuration, crack propagation intersected individual deposited roads, demonstrating that failure was not restricted to interlayer regions. In the −45°/45° configuration, the fracture path extended through the inclined filament pattern, resulting in surfaces with fewer distinct interlayer planes. These features suggest a shift in the failure mode from interface-dominated fracture to fracture involving the filament volume.

3.3. Four-Point bending tests

Prior to conducting four-point bending tests, the hardness and void percentage of the printed specimens were evaluated. The results closely aligned with those observed for the tensile test specimens, showing a variation of only 1.3%. Figure 9 graphically presents the values obtained for flexural modulus, flexural strength, and fracture toughness (K_{IC}).

For PLA/Wood without thermal treatment, the flexural modulus was 2.38 GPa for the 0°/90° orientation and 2.83 GPa for the −45°/45° orientation, representing an 18.9% increase for the inclined raster configuration. The incorporation of wood particles reduces the flexural rigidity of the composite, since the particles act as discontinuities in the PLA matrix and restrict load transfer between layers. This behavior has been reported in the study by Mazzanti et al.[27], indicating that the inclusion of wood particles decreases the flexural modulus due to interfacial incompatibility and localized stress concentration. This effect is more evident in the 0°/90° orientation, where bending loads induce separation along interlayer boundaries, revealing adhesion as the main limitation. In contrast, the −45°/45° orientation distributes bending stresses along inclined filament paths, reducing stress localization at layer interfaces and resulting in higher

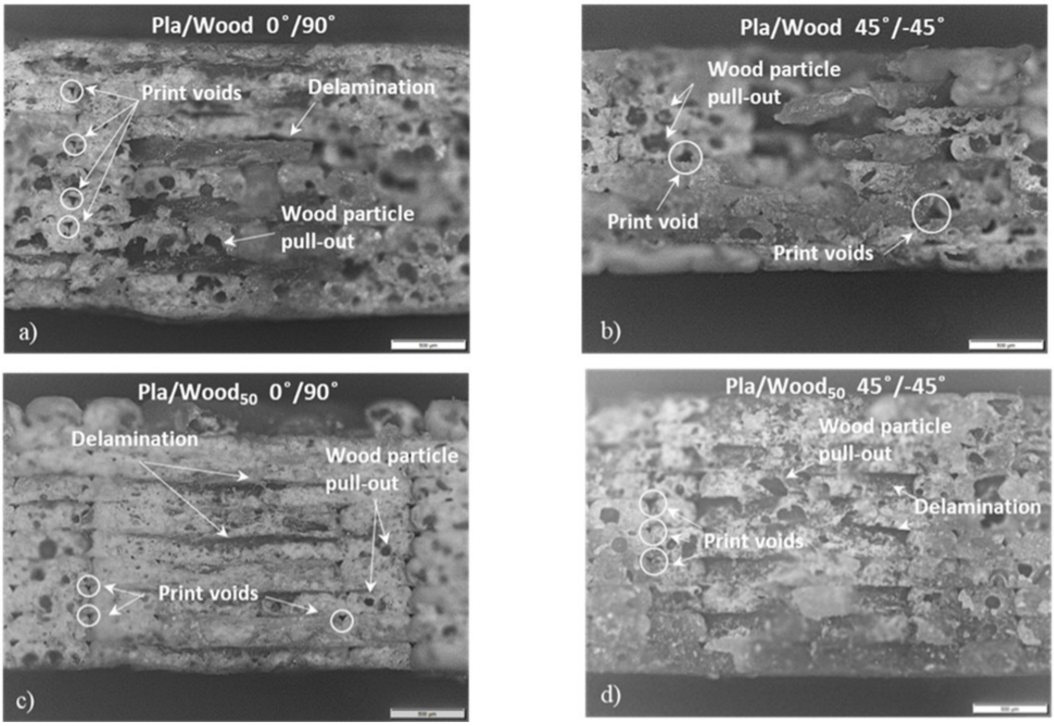

Figure 8. Cross-sectional views of fracture regions in PLA/Wood tensile specimens by printing orientation and heat treatment, (a) PLA/Wood 0º/90º, (b) PLA/Wood -45º/45º, (c) PLA/Wood$_{50}$ 0º/90º, (d) PLA/Wood$_{50}$ -45º/45º.

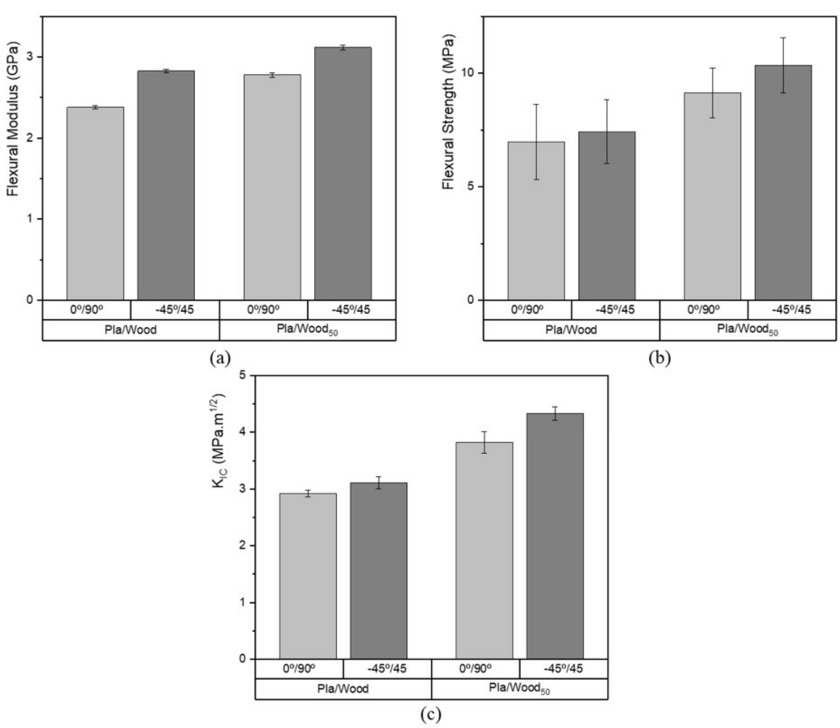

Figure 9. (a) Flexural Modulus, (b) Flexural Strength, and (c) Fracture Toughness (K_{IC}) results.

flexural stiffness, consistent with the interlayer reinforcement mechanism described by Çakan[28].

For PLA/Wood$_{50}$, annealing at 50 °C increased the flexural modulus to 2.78 GPa in the 0°/90° orientation and 3.12 GPa in the −45°/45° orientation, corresponding to gains of 16.8% and 10.2%, respectively, compared to the untreated condition. The heat treatment reduced internal stress gradients and promoted continuity between deposited layers. Similar findings were reported in the study by Wach et al.[29], indicating that moderate annealing increases flexural stiffness by enhancing interlayer cohesion. The −45°/45° configuration exhibited a higher modulus because the bending load is transmitted partly through shear between adjacent filaments, making the mechanical response dependent on the integrity of the interlayer interfaces.

The flexural strength of untreated PLA/Wood was 6.98 MPa for the 0°/90° orientation and 7.43 MPa for the −45°/45° orientation, representing an increase of +6.4% for the inclined raster configuration. The presence of wood particles generates stress concentration regions at the PLA–wood interfaces due to the difference in stiffness and surface energy. A similar effect was reported by Fouly et al.[23], where rigid wood inclusions created heterogeneous stress fields that limited flexural strength in PLA-based composites. In the −45°/45° orientation, the inclined filament paths allow bending loads to be transmitted through combined tension and shear between adjacent filaments, producing higher apparent strength under flexural loading.

After annealing at 50 °C, the flexural strength reached 9.14 MPa in the 0°/90° orientation and 10.35 MPa in the −45°/45° orientation, corresponding to increases of 30.9% and 39.3%, respectively, compared to the untreated condition. These changes are attributed to the relaxation of residual stresses and the closer contact between adjacent extruded filaments, which reduces the number and size of interfacial voids. A comparable strengthening effect was described in the study by Fouly et al.[23], indicating that post-printing heat treatment improves both flexural and tensile strength through stress relaxation and increased layer adhesion. Under these conditions, stress transmission between printed layers occurs with greater continuity. The −45°/45° orientation exhibited the highest strength due to the combined action of tensile and shear components along the inclined filament paths, making this configuration particularly responsive to thermal treatment.

The fracture toughness (K_{IC}) exhibited orientation-dependent behavior. For untreated PLA/Wood, the values were 2.92 MPa√m in the 0°/90° orientation and 3.11 MPa√m in the −45°/45° orientation, representing an increase of +6.5% for the inclined raster configuration. The incorporation of wood particles disrupts the polymer matrix continuity and creates preferential regions for crack initiation, reducing resistance to crack propagation. In the −45°/45° orientation, the inclined filament paths deflect the fracture plane, causing the crack to follow a non-linear trajectory that demands greater energy for propagation.

After annealing at 50 °C, the fracture toughness increased to 3.82 MPa√m in the 0°/90° orientation and 4.33 MPa√m in the −45°/45° orientation, corresponding to gains of 30.8% and 39.2%, respectively, relative to the untreated condition. Similar improvements in toughness resulting from annealing were reported in the study by Park et al.[30], indicating that moderate annealing promotes microstructural densification and reduces crack propagation paths. The higher K_{IC} observed in the −45°/45° orientation suggests that fracture propagation along inclined filament paths requires greater energy dissipation, highlighting the combined influence of annealing and raster arrangement on fracture resistance.

3.3.1. Fracture analysis

For PLA/Wood specimens without thermal treatment printed in the 0º/90° orientation, fracture occurred along interlayer boundaries. This corresponds to the measured flexural strength of 6.98 MPa and K_{IC} of 2.92 MPa√m, indicating limited stress transfer between adjacent filament roads. The presence of wood particles disrupts the continuity of the PLA matrix and creates localized crack initiation sites, which promotes fracture propagation along layer interfaces. Similar behavior has been reported by Mazzanti et al.[27] and by Park et al.[30], both of which demonstrated interfacial fracture and poor stress transfer along interlayer boundaries in PLA/wood systems.

In contrast, untreated PLA/Wood specimens printed in the −45°/45° orientation exhibited a flexural strength of 7.43 MPa and a K_{IC} of 3.11 MPa√m, and the fracture surfaces showed reduced interlayer separation. The inclined raster arrangement distributed bending stresses through a combination of axial and shear components, decreasing the stress concentration at layer interfaces. Under these conditions, crack propagation occurred along a longer, non-linear trajectory across the printed layers, extending the fracture path before failure. This fracture pattern demonstrates that the −45°/45° orientation enables efficient stress transfer between adjacent extruded filaments during bending, consistent with the observations of Ziemian et al.[31] and Popescu et al.[32].

The comparison between printing orientations highlights the central role of raster angle in defining structural cohesion in PLA/Wood composites. The −45°/45° orientation offers improved interlayer connectivity under flexural loading, while the 0°/90° configuration tends to concentrate stresses along planar interfaces that separate deposited layers. Therefore, printing orientation is a decisive factor in determining fracture mode and overall structural robustness, particularly in applications subject to repeated bending or dynamic stresses. This anisotropic behavior agrees with the findings of Torrado and Roberson[33].

After annealing at 50 °C, the fracture surfaces of PLA/Wood$_{50}$ specimens exhibited fewer interlayer separations and reduced crack branching at the interfaces compared to the untreated condition. This behavior aligns with the increases measured in flexural modulus (from 2.78 to 3.12 GPa) and flexural strength (from 9.14 to 10.35 MPa). The heat treatment relieved residual stresses within the printed strands and improved the contact between adjacent deposited paths, allowing stable load transfer across layer boundaries during bending. Comparable effects were reported in the studies by Fouly et al.[23] and by Kahya et al.[24], indicating that moderate annealing reduces delamination and enhances interlayer cohesion in printed PLA structures.

Fracture resistance in PLA/Wood depends on the interaction between raster architecture and interlayer bonding. The higher K_{IC} measured for neat PLA in the 0°/90° orientation, relative to PLA/Wood in −45°/45°, indicates that the addition of wood particles reduces toughness by introducing discontinuous interfaces and stress concentrators within the matrix. Consequently, both the material system and the printing orientation must be selected with attention to crack initiation and propagation paths. Annealing at 50 °C increased interlayer adhesion and preserved part geometry, which coincides with the gains observed in flexural and fracture metrics. These mechanisms are consistent with the microstructural findings reported in the study by Wach et al.[29] indicating that thermal annealing slightly below the glass transition temperature promotes denser lamellar arrangements and delays crack propagation in PLA-based systems.

For untreated PLA/Wood printed at 0°/90° (Figure 10a), the fracture surface shows separation between adjacent deposited layers and the presence of microcrack paths. This morphology corresponds to the flexural modulus of 2.38 GPa and flexural strength of 6.98 MPa measured for this condition. The layer separation indicates limited stress transfer across interfacial regions during bending. In addition, the presence of wood particles interrupts the continuity of the PLA matrix, creating local stiffness variations that facilitate crack initiation and propagation.

In contrast, untreated PLA/Wood printed at −45°/45° (Figure 10b) exhibited less pronounced delamination, with fracture paths propagating through inclined raster lines rather than strictly along interlayer boundaries. This behavior correlates with the slightly higher flexural modulus (2.83 GPa) and flexural strength (7.43 MPa) measured for this orientation. The −45°/45° raster arrangement promotes a uniform stress distribution, delaying crack propagation and producing a tortuous fracture surface that indicates greater energy dissipation before failure.

After annealing at 50°C, microstructural changes are observed in both orientations. For PLA/$Wood_{50}$ printed at 0°/90° (Figure 10c), the fracture surfaces show reduced interlayer separation and fewer microcracks compared to untreated material. This is consistent with the increases in flexural modulus to 2.78 GPa and flexural strength to 9.14 MPa, reflecting enhanced interlayer adhesion and relaxation of internal residual stresses induced by the heat treatment.

For PLA/$Wood_{50}$ printed at −45°/45° (Figure 10d), the fracture surface exhibited minimal delamination and stable failure paths across layers. This condition corresponds to the highest flexural modulus (3.12 GPa) and flexural strength (10.35 MPa) among the tested configurations. Annealing at 50 °C promoted closer contact between PLA chains and wood particles, reducing voids and improving stress transmission

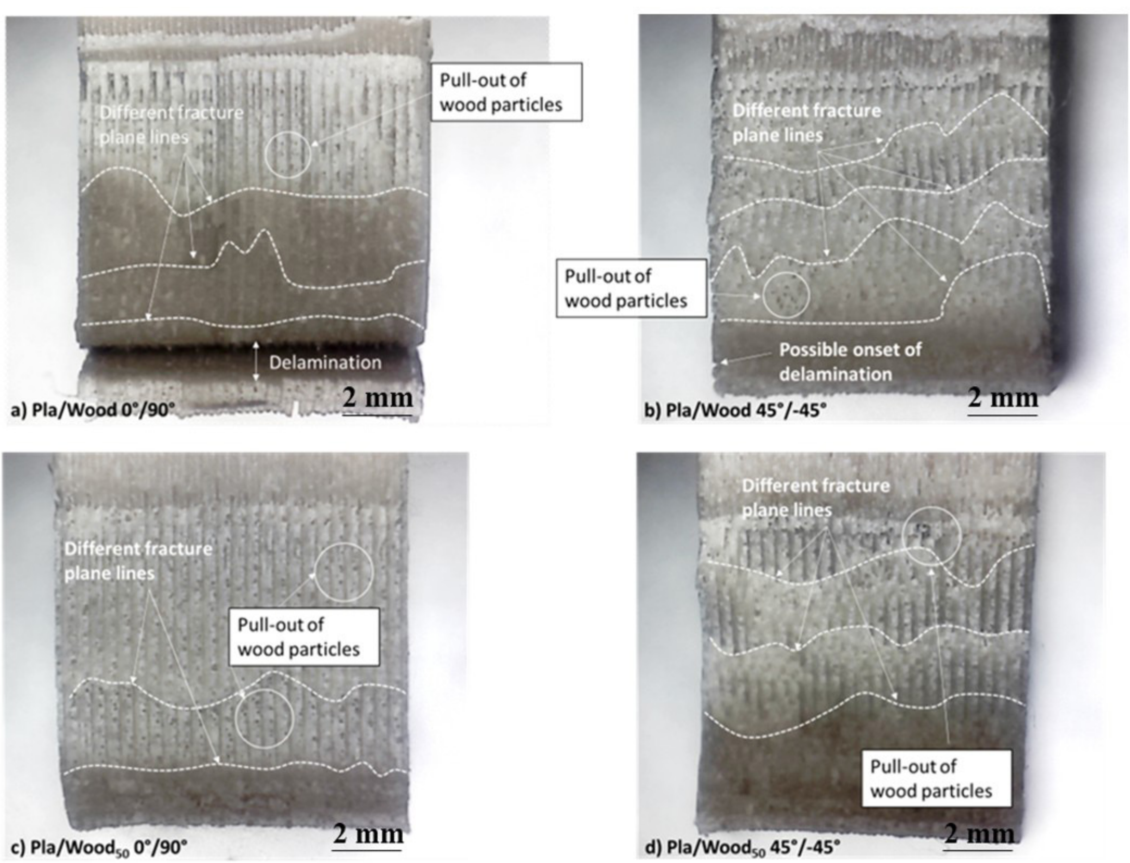

Figure 10. Micrographs of fracture cross-sections of specimens after four-point bending test, (a) PLA/Wood 0º/90º, (b) PLA/Wood -45º/45º, (c) PLA/$Wood_{50}$ 0º/90º, (d) PLA/$Wood_{50}$ -45º/45º.

across layers, which increased resistance to crack initiation and propagation.

The results indicate that the −45°/45° orientation distributes bending stresses through a combination of tensile and shear components, reducing localized stress at interlayer boundaries. Annealing at 50 °C improved interlayer contact and reduced microstructural discontinuities, as supported by microscopy and mechanical data. The combined effect of raster orientation and heat treatment increased resistance to crack initiation and propagation during flexural loading in the PLA/Wood composite. Similar conclusions were presented in the study by Rodríguez-Panes et al.[34], indicating that inclined raster orientations enhance interlayer shear transfer and delay fracture propagation under bending loads.

3.4. Impact resistance (charpy test)

Before conducting the Charpy impact tests, Shore D hardness and void percentage were measured for all printed specimens, and the results were within 1.6% of the values obtained for the tensile specimens. This confirmed that the printed parts had comparable density and consolidation, ensuring that differences observed in the impact response were due to printing orientation and annealing, rather than variations in specimen fabrication. Figure 11 presents the measured impact resistance and tensile toughness for each printing orientation, both before and after annealing.

For untreated PLA/Wood, the impact resistance was 34.36 kJ/m^2 in the 0°/90° orientation and 42.23 kJ/m^2 in the −45°/45° orientation, representing an increase of approximately 22.9% for the inclined raster configuration. The lower energy absorption capacity compared to homogeneous PLA materials is associated with the presence of wood particles, which act as stress concentrators and promote interlaminar fracture. In composites produced via FDM, these regions become preferential sites for crack initiation and propagation, reducing the ability to dissipate impact energy. This effect has been reported in the studies by Mazzanti et al.[27], indicating that wood inclusions reduce impact energy absorption due to particle–matrix incompatibility and microvoid formation, and that interlayer fracture is associated with insufficient wetting of wood particles by the PLA matrix.

The behavior of tensile toughness aligns with the impact resistance trends. Untreated PLA/Wood exhibited toughness values of 0.429 J/cm^3 (0°/90°) and 0.527 J/cm^3 (−45°/45°), while annealed PLA/Wood50 reached 0.610 J/cm^3 and 0.679 J/cm^3, respectively. These values represent increases of 42.2% for the 0°/90° orientation and 28.8% for the −45°/45° orientation after annealing. These results confirm that annealing increases cohesive strength between layers, reduces localized strain concentration, and improves the material's ability to absorb deformation energy prior to fracture. Similar observations were presented in the study by Fouly et al.[23], signifying that moderate annealing enhances impact toughness and strain energy absorption in printed PLA through stress relaxation and improved interlayer bonding.

The difference in tensile toughness between printing orientations also reflects the influence of raster arrangement on deformation behavior. For the untreated condition, the 0°/90° and −45°/45° orientations exhibited values of 0.429 J/cm^3 and 0.527 J/cm^3, respectively, corresponding to a difference of 23%. After annealing at 50 °C, the toughness values increased to 0.610 J/cm^3 (0°/90°) and 0.679 J/cm^3 (−45°/45°), reducing the difference between orientations to 11.3%. The reduction in variation suggests that heat treatment decreased the anisotropy typically associated with FDM by improving the continuity of load transmission across deposited layers. This result is consistent with the trend observed in impact resistance measurements and with the findings presented in the study by Rodríguez-Panes et al.[34], demonstrating that inclined raster orientations enhance the capacity for energy dissipation under dynamic loading.

Figure 12 presents the fracture surfaces obtained after the Charpy impact tests for both printing orientations and thermal conditions. For untreated PLA/Wood printed at −45°/45° (Figure 12b), the fracture surfaces show multiple separation planes along the deposited layers. The inclined raster arrangement positions the interfaces at an angle with respect to the impact direction, enabling cracks to follow the interlayer boundaries during propagation. In this condition, failure proceeds primarily by interlaminar separation, indicating that the interfaces between layers govern the fracture process under impact loading. This behavior is consistent with the microstructural analysis presented in the study by Popescu et al.[32], which indicates that raster inclination directly affects crack trajectory and interlayer delamination under impact.

In untreated PLA/Wood printed at 0°/90° (Figure 12a), the fracture surface displays fewer interlayer separation

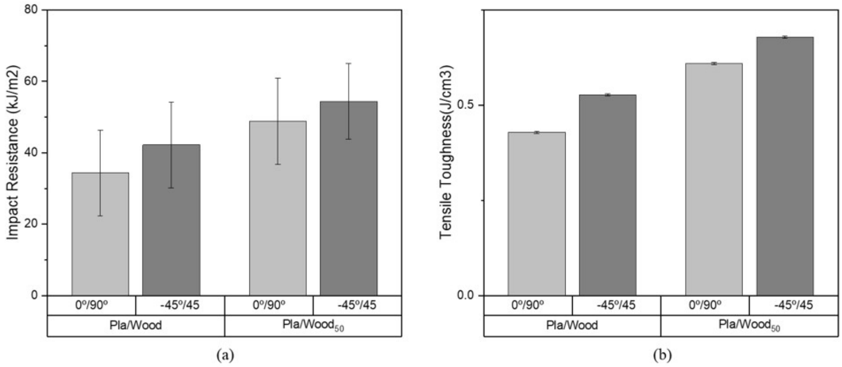

Figure 11. Impact resistance and tensile toughness results.

planes compared to the −45°/45° configuration. The deposited filaments in this orientation are arranged approximately parallel to the impact loading direction, which constrains crack propagation to proceed through the material rather than along layer boundaries. Under these conditions, fracture develops through the printed strands, and separation between adjacent layers is less pronounced.

After annealing at 50 °C, both printing orientations exhibited a reduction in visible interlayer separation, as shown in Figures 12c and 12d. The fracture surfaces display fewer planes associated with delamination, and crack propagation proceeds with fewer deviations along layer boundaries. In the −45°/45° configuration, the decrease in interlaminar separation is more apparent compared to the untreated condition, suggesting that the thermal treatment limits crack propagation along the layer interfaces that were previously more prone to separation. This improvement is consistent with the results reported in the study by Kahya et al.[24], indicating that annealing reduces interfacial voids and delamination in printed PLA parts.

Overall, the fracture surfaces indicate that the printing orientation influences the dominant crack path and that annealing at 50 °C reduces interlayer separation. This reduction in interfacial discontinuities is consistent with the increases in impact resistance and tensile toughness observed after heat treatment. Similar conclusions were presented in the study by Wach et al.[29], signifying that thermal annealing promotes lamellar densification and increases energy dissipation during impact.

3.5. ANOVA

To assess the effect of annealing and printing orientation on the measured properties, a two-way ANOVA was applied to all mechanical responses (hardness, void fraction, tensile properties, flexural properties, impact resistance, and tensile toughness). The fixed factors were annealing condition (untreated vs. 50 °C) and printing orientation (0°/90° vs. −45°/45°), and the interaction term between these factors was included. All tests used $n = 5$ specimens per condition, and statistical significance was considered at $\alpha = 0.05$. The ANOVA identifies the contribution of each factor and of their interaction to the response variance. The corresponding F-values, p-values, and model R^2 values are summarized in the following tables. Table 2 presents the ANOVA results for Shore D hardness and void fraction.

The ANOVA results show that both annealing and printing orientation have statistically significant effects on Shore D hardness and void content. For Shore D, printing orientation presented the highest influence ($F = 203.15$, $p < 10^{-10}$), followed by annealing ($F = 57.25$, $p < 10^{-6}$). This indicates

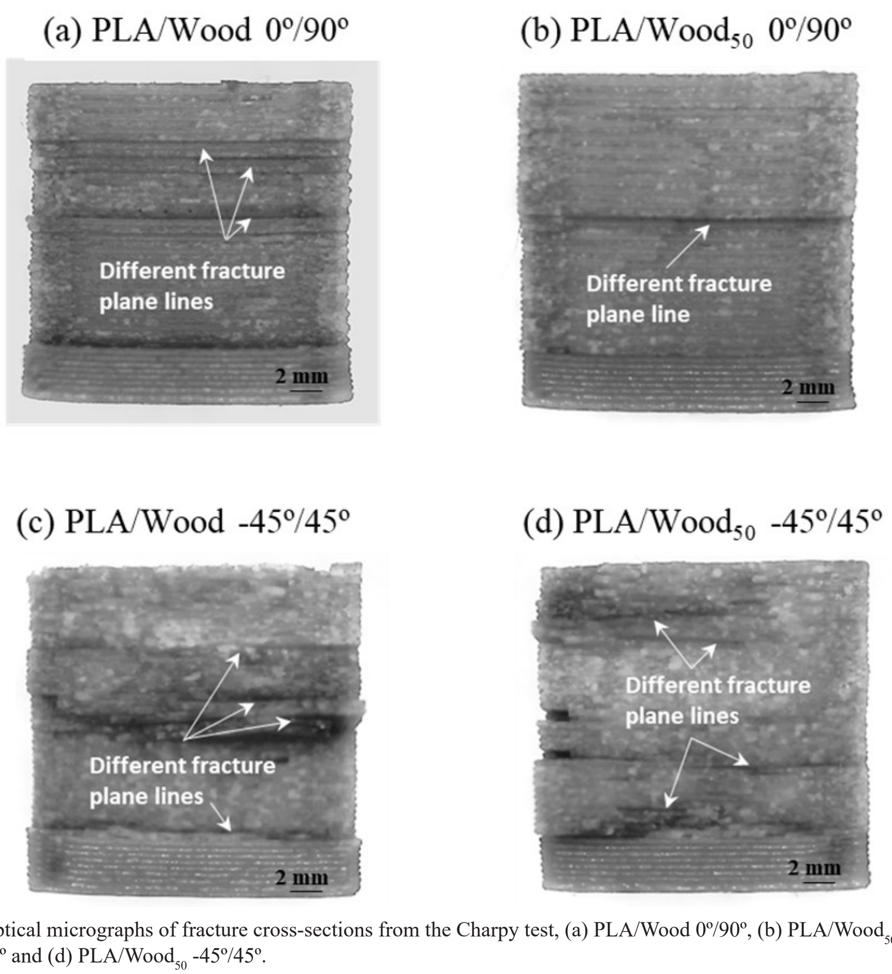

Figure 12. Optical micrographs of fracture cross-sections from the Charpy test, (a) PLA/Wood 0º/90º, (b) PLA/Wood$_{50}$ 0º/90º, (c) PLA/Wood -45º/45º and (d) PLA/Wood$_{50}$ -45º/45º.

that hardness is influenced by the geometric arrangement of deposited layers. The 0°/90° orientation produces layer alignment parallel to the indentation direction, which increases resistance to local deformation. In contrast, the −45°/45° orientation introduces inclined interfaces that exhibit lower resistance under the same loading condition. The increase in hardness after annealing at 50 °C is consistent with the reduction of internal residual stresses and the densification of contact regions between deposited strands, leading to a surface with reduced compliance during indentation.

For void content, annealing was the dominant factor ($F = 126.04$, $p < 10^{-9}$), whereas printing orientation also influenced the response ($F = 12.08$, $p = 3.12\times10^{-3}$). The reduction in void percentage after annealing indicates that heating near the transition region allows polymer chains to rearrange within interlayer regions, reducing the size and continuity of internal gaps. This rearrangement increases the degree of contact between adjacent deposited filaments. The interaction term between annealing and orientation was not statistically significant for either hardness ($p = 0.408$) or void percentage ($p = 0.778$), indicating that the effect of annealing was independent of raster orientation.

The determination coefficients ($R^2 = 0.93$ for Shore D and $R^2 = 0.88$ for void%) indicate that annealing and printing orientation account for most of the variation observed in these properties. This statistical outcome aligns with the microstructural evidence, in which annealed specimens present reduced interlayer discontinuities. The analysis also shows that annealing at 50 °C affects interlayer contact without altering the printed geometry, while raster orientation continues to influence the surface-level mechanical response. Table 3 presents the ANOVA results for tensile modulus, tensile strength, and strain, highlighting the contribution of annealing and layer orientation to the mechanical response of the composite.

For Young's modulus, both annealing and printing orientation are significant, with large F-values and $p < 10^{-10}$. The increase in modulus after annealing at 50 °C is consistent with stress relaxation and improved interlayer contact, while the 0°/90° raster provides a more efficient load path than −45°/45°. The interaction term is not significant, indicating that the annealing effect does not depend on the chosen orientation. The model explains 96.9% of the variance, which is compatible with the strong factor effects and with the microstructural evidence of reduced interlayer gaps.

For tensile strength, annealing is the dominant factor ($F \approx 1284$, $p \ll 0.001$), followed by orientation ($F \approx 16.3$, $p < 0.001$). The lack of interaction again shows that the gain due to annealing is stable across rasters. The coefficient of determination is 98.8%, indicating that the two factors account for almost all variability observed in strength, in line with the large experimental increments reported after heat treatment and the improved interfacial bonding seen in microscopy.

For strain at break, none of the terms reaches $p < 0.05$; orientation is borderline ($p \approx 0.067$). The low R^2 ($\approx 33\%$) reflects the higher intrinsic dispersion of strain in FDM composites and the competing effects of local densification and constraint introduced by wood particles. This outcome is consistent with the mixed trends observed in ductility and does not contradict the clear factor effects seen in modulus and tensile strength. Table 4 reports the ANOVA analysis

Table 2. ANOVA Results – Shore D Hardness and Void Fraction.

Source of variation	Shore D		Void %	
	F-value	p-value	F-value	p-value
Annealing	57.25	1.13×10^{-6}	126.04	5.37×10^{-9}
Orientation	203.15	1.64×10^{-10}	12.08	3.12×10^{-3}
Annealing × Orientation	0.72	0.408	0.08	0.778
R^2	0.93 (93%)		0.88 (88%)	

Table 3. ANOVA Results – Tensile Test.

Source of variation	Young's Modulus		Tensile Strength		Strain at break	
	F-value	p-value	F-value	p-value	F-value	p-value
Annealing	239.7122	4.75×10^{-11}	1284.0214	1.11×10^{-16}	1.6701	0.2146
Orientation	265.8017	2.18×10^{-11}	16.3079	9.52×10^{-4}	3.8634	0.0670
Annealing × Orientation	1.6900	0.2120	0.0314	0.8616	2.3310	0.1463
R^2	0.9694 (96.94%)		0.9878 (98.78%)		0.3295 (32.95%)	

Table 4. ANOVA Results Four-Point Bending.

Source of variation	Flexural Modulus		Flexural Strength		K_{IC}	
	F-value	p-value	F-value	p-value	F-value	p-value
Annealing	312.45	< 0.001	42.78	< 0.001	188.63	< 0.001
Orientation	528.39	< 0.001	6.91	0.014	31.74	< 0.001
Annealing × Orientation	4.22	0.057	2.48	0.134	2.17	0.152
R^2	0.982 (98.2%)		0.874 (87.4%)		0.941 (94.1%)	

Table 5. ANOVA Results Charpy Test.

Source of variation	Impact Resistance		Tensile Toughness	
	F-value	p-value	F-value	p-value
Annealing	6.85	0.016	907.42	<0.0001
Orientation	2.17	0.159	1822.65	<0.0001
Annealing × Orientation	0.64	0.432	3.26	0.086
R^2	0.45 (45%)		0.999 (99.9%)	

for impact resistance and tensile toughness, examining how annealing and raster orientation influence energy absorption behavior.

For the flexural modulus, both annealing and printing orientation exhibit strong factor effects ($p < 0.001$). Annealing at 50 °C increases stiffness due to reduced interlayer voids and enhanced matrix–particle contact, while The −45°/45° orientation provides a different load transfer path consistent with the higher modulus measured for this raster. The high R^2 (≈98%) reflects the clear sensitivity of modulus to structural consolidation.

For flexural strength, annealing significantly improves resistance to bending, while the effect of orientation is smaller but still statistically significant ($p \approx 0.014$). The interaction term is not significant, indicating that the benefit of annealing is consistent across raster configurations. The R^2 of 87% indicates that flexural strength depends both on structural parameters and local defect distribution.

For K_{IC}, annealing and orientation both show strong effects ($p < 0.001$), indicating that fracture resistance is sensitive to interlayer adhesion and stress redistribution mechanisms. The high R^2 (≈94%) aligns with the improved continuity of fracture surfaces observed microscopically in PLA/Wood50, especially in the −45°/45° condition. The ANOVA results for impact resistance and tensile toughness are summarized in Table 5.

Annealing produced a statistically significant effect on both properties ($p < 0.05$), confirming that heat treatment at 50 °C effectively enhances energy absorption capacity. In contrast, the printing orientation did not significantly influence impact resistance ($p > 0.05$), likely due to the higher variability inherent to impact fracture processes. For tensile toughness, however, orientation was statistically significant ($p < 0.0001$), indicating that layer arrangement strongly governs the energy dissipation mechanisms during tensile deformation. The interaction between annealing and orientation was not statistically significant for either property ($p > 0.05$), suggesting that the beneficial effect of annealing is consistent for both 0°/90° and −45°/45° configurations. The coefficient of determination was high for tensile toughness ($R^2 = 0.999$), indicating an excellent model fit, whereas impact resistance presented moderate correlation ($R^2 = 0.45$), reflecting its larger experimental variability.

When comparing the untreated and annealed conditions, the relative difference between the 0°/90° and −45°/45° orientations decreased for tensile strength, flexural properties, impact resistance, and tensile toughness. This indicates that the heat treatment reduced the sensitivity of the mechanical response to raster direction. The treatment at 50 °C promoted closer contact between adjacent deposited filaments and reduced the connectivity of voids, which improved stress transfer across interlayer boundaries. As a result, mechanical behavior became less dependent on the specific layer arrangement, reflecting a reduction in anisotropy inherent to the FDM process. This effect is consistent with the fracture observations, where annealed specimens exhibited more continuous failure paths and reduced interlayer separation.

In addition to the experimental framework employed herein, the approach could be augmented by computational modelling techniques to deepen the mechanistic understanding of annealing-induced changes in PLA/wood composites. For example, mesh-free particle methods such as described by Rabczuk and Belytschko[35] enable simulation of microstructural evolution, crack initiation and propagation without the constraints of remeshing. The energy-based machine-learning framework presented by Samaniego et al.[36] integrates partial-differential-equation formalisms and data-driven modelling to yield predictive insight and uncertainty quantification. Future work could integrate such methods to simulate the kinetics of filament bonding, void closure and crystallisation during annealing at 50 °C, thereby linking observed experimental trends with an underlying physics-based model.

4. Conclusions

The heat treatment at 50 °C increased the tensile strength of PLA/Wood from 17.83 MPa to 28.95 MPa in the 0°/90° orientation and from 16.55 MPa to 27.58 MPa in the −45°/45° orientation. The Young's modulus also increased, from 3.23 GPa to 3.41 GPa in the 0°/90° condition and from 3.05 GPa to 3.21 GPa in the −45°/45° condition. The strain at maximum load was maintained in the 0°/90° orientation (approximately 5–6%) and increased from 0.0579 to 0.0679 in the −45°/45° orientation. These results correspond to stress relaxation and improved interlayer bonding during thermal exposure.

The −45°/45° orientation showed higher flexural strength after annealing (10.35 MPa) compared to the 0°/90° configuration (9.14 MPa), reflecting the influence of raster inclination on the distribution of bending stresses. The flexural modulus also increased after heat treatment, from 2.38 GPa to 2.78 GPa in the 0°/90° orientation and from 2.83 GPa to 3.12 GPa in the −45°/45° orientation, indicating improved contact between adjacent deposited strands.

The fracture toughness (KIC) increased from 2.92 MPa√m to 3.82 MPa√m in the 0°/90° orientation and from 3.11 MPa√m to 4.33 MPa√m in the −45°/45° orientation. The tensile toughness also increased, from 0.429 J/cm^3 to 0.610 J/cm^3 in the 0°/90° configuration and from 0.527 J/cm^3 to 0.679 J/cm^3 in the −45°/45° configuration. These results indicate greater resistance to crack initiation and higher energy absorption capacity under quasi-static and impact loading.

The void content decreased to 11.48% in the 0°/90° specimens and to 11.42% in the −45°/45° specimens after annealing, accompanied by an average increase of approximately 2% in Shore D hardness. These observations indicate reduced interlayer gaps and increased surface consolidation.

Fracture analysis showed that annealed specimens displayed less interlayer separation and more continuous fracture surfaces in both orientations. Overall, the combined effect of raster arrangement and heat treatment at 50 °C contributed to improved structural cohesion and mechanical response in PLA/Wood composites without altering external geometry.

5. Acknowledgments

The authors would like to thank the Postgraduate Program in Mechanical Engineering of the Federal University of Minas Gerais (UFMG), Brazil, for the provision of laboratory facilities.

This work was partly financed by the Coordenação de Aperfeiçoamento de Pessoal de Nível Superior (CAPES)–Finance Code 001. Also, it must be acknowledged the financial support of the Conselho Nacional de Desenvolvimento Científico e Tecnológico (CNPq) and Fundação de Amparo à Pesquisa do Estado de Minas Gerais (FAPEMIG).

6. References

1. Gao W, Zhang Y, Ramanujan D, Ramani K, Chen Y, Williams CB, et al. The status, challenges, and future of additive manufacturing in engineering. Comput Aided Des. 2019;69:65-89. https://doi.org/10.1016/j.cad.2015.04.001.
2. Ngo TD, Kashani A, Imbalzano G, Nguyen KTQ, Hui D. Additive manufacturing (3D printing): A review of materials, methods, applications and challenges. Compos, Part B Eng. 2018;143:172-96. https://doi.org/10.1016/j.compositesb.2018.02.012.
3. Rajeshkumar G, Seshadri SA, Devnani GL, Sanjay MR, Siengchin S, Maran JP, et al. Environment friendly, renewable and sustainable poly lactic acid (PLA) based natural fiber reinforced composites – A comprehensive review. J Clean Prod. 2021;310:127483. https://doi.org/10.1016/j.jclepro.2021.127483.
4. Ma T, Zhang Y, Ruan K, Guo H, He M, Shi X, et al. Advances in 3D printing for polymer composites: A review. InfoMat. 2024;6(6):e12568. https://doi.org/10.1002/inf2.12568.
5. Alkabbanie R, Aktas B, Demircan G, Yalcin S. Short carbon fiber-reinforced PLA composites: influence of 3D-printing parameters on the mechanical and structural properties. Iran Polym J. 2024;33(8):1065-74. https://doi.org/10.1007/s13726-024-01315-8.
6. Siddiqui VU, Yusuf J, Sapuan SM, Hasan MZ, Mudah Bistari MM, Mohammadsalih ZG. Mechanical properties and flammability analysis of wood fiber filled Polylactic Acid (PLA) composites using additive manufacturing. J Nat Fibers. 2024;21(1):1-17. https://doi.org/10.1080/15440478.2024.2409868.
7. Fabra AP, De Castro Magalhães F, Campos Rubio J. Experimental characterization of PLA composites printed by fused deposition modelling. J Compos Mater. 2023;57(5):941-54. https://doi.org/10.1177/00219983221146619.
8. Maziero R, Cavalcanti WM, Castro BD, et al. Novel green composite material manufactured by extrusion process from recycled polypropylene matrix reinforced with eucalyptus fibres and granite powder. Advances in Materials Research (South Korea). 2023;12(2):119-31. https://doi.org/10.12989/amr.2023.12.2.119.
9. Sanjay MR, Madhu P, Jawaid M, Senthamaraikannan P, Senthil S, Pradeep S. Characterization and properties of natural fiber polymer composites: A comprehensive review. J Clean Prod. 2018;170:566-81. https://doi.org/10.1016/j.jclepro.2017.10.101.
10. Narlioglu N. Effect of printing speed on the mechanical properties and thermal properties of wood–PLA composite filament. Furniture and Wooden Material Research Journal. 2024;7(1):97-106. https://doi.org/10.33725/mamad.1486558.
11. Le Duigou A, Castro M, Bevan R, Martin N. Additive manufacturing of wood-based materials for biocomposites and architectural applications. Front Mech Eng. 2019;5:35.
12. Pavlovic A, Valzania L, Minak G. Effects of moisture absorption on the mechanical and fatigue properties of natural fiber composites: a review. Polymers. 2025;17(14):1996. https://doi.org/10.3390/polym17141996.
13. Hill C, Altgen M, Penttilä P, Rautkari L. Review: interaction of water vapour with wood and other hygro-responsive materials. J Mater Sci. 2024;59(18):7595-635. https://doi.org/10.1007/s10853-024-09636-y.
14. Ahn SH, Montero M, Odell D, Roundy S, Wright PK. Anisotropic material properties of fused deposition modeling ABS. Rapid Prototyping J. 2002;8(4):248-57. https://doi.org/10.1108/13552540210441166.
15. Wickramasinghe S, Do T, Tran P. FDM-based 3D printing of polymer and associated composite: a review on mechanical properties, defects and treatments. Polymers. 2020;12(7):1529. https://doi.org/10.3390/polym12071529.
16. Le Duigou A, Castro M, Bevan R, Martin N. 3D printing of biocomposites: A review. Compos, Part A Appl Sci Manuf. 2019;124:105-15.
17. Kariz M, Sernek M, Kuzman MK. Use of wood powder and PLA in 3D printing. Mater Manuf Process. 2019;31(5):552-7.
18. Kartal F, Kaptan A. Effects of annealing temperature and duration on mechanical properties of PLA plastics produces by 3D Printing. European Mechanical Science. 2023;7(3):152-9. https://doi.org/10.26701/ems.1290961.
19. Jayanth N, Jaswanthraj K, Sandeep S, Mallaya NH, Siddharth SR. Effect of heat treatment on mechanical properties of 3D printed PLA. J Mech Behav Biomed Mater. 2021;123:104764. https://doi.org/10.1016/j.jmbbm.2021.104764.
20. Issametova M, Martyushev N, Zhastalap A, Sabirova LB, Assemgul U, Tursynbayeva A, et al. Determination of residual stresses in 3D-Printed polymer parts. Polymers. 2024;16(14):2067. https://doi.org/10.3390/polym16142067.
21. Suder J, Bobovsky Z, Mlotek J, Vocetka M, Zeman Z, Safar M. Experimental analysis of temperature resistance of 3d printed pla components. MM Sci J. 2021;1(1):4322-7. https://doi.org/10.17973/MMSJ.2021_03_2021004.
22. Tomec DK, Schwarzkopf M, Repic R, Žigon J, Gospodarič B, Kariž M. Effect of thermal modification of wood particles for wood-PLA composites on properties of filaments, 3D-printed parts and injection moulded parts. Holz Roh- Werkst. 2024;82(2):403-16. https://doi.org/10.1007/s00107-023-02018-2.
23. Fouly A, Albahkali T, Abdo HS, Salah O. Investigating the mechanical properties of annealed 3D-printed PLA–date pits composite. Polymers. 2023;15(16):3395. https://doi.org/10.3390/polym15163395.
24. Kahya Ç, Tunçel O, Çavusoglu C, Tüfekci K. Thermal annealing optimization for improved mechanical performance of PLA parts produced via 3D printing. Polym Test. 2025;144:108735. https://doi.org/10.1016/j.polymertesting.2025.108735.
25. Natayu A, Muhammad AA, Tumada A, Saptaji K, Trisnadewi T, Triawan F, et al. Effect of annealing on the mechanical properties of fused deposition modeling 3d printed PLA. Journal Rekayasa Mesin. 2024;15(3):1343-51. https://doi.org/10.21776/jrm.v15i3.1625.
26. Shbanah M, Jordanov M, Nyikes Z, Tóth L, Kovács TA. The Effect of heat treatment on a 3D-printed PLA polymer's mechanical properties. Polymers. 2023;15(6):1587. https://doi.org/10.3390/polym15061587.

27. Mazzanti V, Malagutti L, Mollica F. FDM 3D printing of polymers containing natural fillers: A review of their mechanical properties. Polymers. 2019;11(7):1094. https://doi.org/10.3390/polym11071094.
28. Çakan BG. Effects of raster angle on tensile and surface roughness properties of various FDM filaments. J Mech Sci Technol. 2021;35(8):3347-53. https://doi.org/10.1007/s12206-021-0708-8.
29. Wach RA, Wolszczak P, Adamus-Wlodarczyk A. Enhancement of mechanical properties of FDM-PLA parts via thermal annealing. Macromol Mater Eng. 2018;303(9):1800169. https://doi.org/10.1002/mame.201800169.
30. Park SD, Todo M, Arakawa K. Effect of annealing on the fracture toughness of poly(lactic acid). J Mater Sci. 2004;39(3):1113-6. https://doi.org/10.1023/B:JMSC.0000012957.02434.1e.
31. Ziemian CW, Ziemian RD, Haile KV. Characterization of stiffness degradation caused by fatigue damage of additive manufactured parts. Mater Des. 2016;109(1/2):209-18. https://doi.org/10.1016/j.matdes.2016.07.080.
32. Popescu D, Zapciu A, Amza C, Baciu F, Marinescu R. FDM process parameters influence over the mechanical properties of polymer specimens: A review. Polym Test. 2018;69:157-66. https://doi.org/10.1016/j.polymertesting.2018.05.020.
33. Torrado A, Roberson DA. Failure analysis and anisotropy evaluation of 3D-printed tensile test specimens of different geometries and print raster patterns. J Fail Anal Prev. 2016;16(1):154-64. https://doi.org/10.1007/s11668-016-0067-4.
34. Rodríguez-Panes A, Claver J, Camacho AM. The influence of manufacturing parameters on the mechanical behaviour of PLA and ABS pieces manufactured by FDM: A comparative analysis. Materials. 2018;11(8):1333. https://doi.org/10.3390/ma11081333.
35. Rabczuk T, Belytschko T. Cracking particles: a simplified meshfree method for arbitrary evolving cracks. Int J Numer Methods Eng. 2004;61(13):2316-43. https://doi.org/10.1002/nme.1151.
36. Samaniego E, Anitescu C, Goswami S, Nguyen-Thanh V, Guo H, Hamdia K, et al. An energy approach to the solution of partial differential equations in computational mechanics via machine learning: Concepts, implementation and applications. Comput Methods Appl Mech Eng. 2020;362:112790. https://doi.org/10.1016/j.cma.2019.112790.

Data Availability

The authors confirm that the data supporting the findings of this study are available within the article.